Journal of the Ceramic Society of Japan 117 [9] 944-949 2009 **Paper**

Fabrication and characterization of $Ni_{0.3}Zn_{0.7}Fe_{2.0}O_4$–$BaTiO_3$ ceramic composites

Kazutomo ABE,† Naoto KITAHARA,* Mikio HIGUCHI and Junichi TAKAHASHI

Division of Materials Chemistry, Graduate School of Engineering, Hokkaido University, Kita-13, Nishi-8, Kita-ku, Sapporo 060−8628
***Faculty of Engineering, Tokyo Polytechnic University, 1583 Iiyama, Atsugi, Kanagawa 243−0297**

The ceramic composites containing 1–25 vol% $BaTiO_3$ in a ferrite matrix phase of $Ni_{0.3}Zn_{0.7}Fe_2O_4$ were fabricated by sintering at 1250°C in air. The sintered composites indicated a steep increase in dielectric permittivity in a small $BaTiO_3$ ratio up to 5 vol%. In a limited $BaTiO_3$ ratio of 3–15 vol%, a reaction between $Ni_{0.3}Zn_{0.7}Fe_2O_4$ and $BaTiO_3$ resulted in the production of a liquid phase during sintering, which caused correspondingly the formation of secondary phases of $BaFe_2O_4$ ss and hexagonal $BaTiO_3$ ss. These solid phase and microstructure changes, however, brought about little contribution to the increasing permittivity of the composites. Electrical property evaluations combined with compositional analysis revealed that the remarkably increasing permittivity could be predominantly attributed to the electron hopping between Fe^{2+} and Fe^{3+} in the ferrite matrix, which was caused by the incorporation of a small amount of Ti^{4+} into the spinel sublattice.

Key-words : $Ni_{0.3}Zn_{0.7}Fe_{2.0}O_4$–$BaTiO_3$ composite, Solid state reaction, Ti-doped NiZn ferrite, Dielectric permittivity, Electromagnetic wave absorber

[Received May 7, 2009; Accepted July 16, 2009]

1. Introduction

Recently, the electric switching power supplies have been widely used in many electronic devices, because of its excellent capability of large electric current generation in a small-sized unit. A very fast switching rate in such a power circuit inevitably results in the generation of emission noise (electromagnetic wave; EM wave) ranging from 0.1 MHz to 10 MHz.[1] The emission noise from switching power supplies equipped in electronic devices causes electromagnetic interference, so-called EMI, between them. In order to suppress the EMI, the emission noise should be shielded or absorbed with some materials.[2),3] Materials such as carbon-ulthane composites[3] and ferrites[3),4] can convert the EM waves (emission noise) to thermal energy by the energy loss characteristics in their electric conduction, dielectric, and/or magnetic properties. Materials having this character are called EM wave absorbers.

The working performance of an EM wave absorber is strongly dependent on the impedance matching between the absorber material and air. Deviation from a condition of the impedance matching between them gives rise to the reflection of EM waves at the surface of the absorber. With Z_0 and Z_1 being an impedance of the air and an EM wave absorber, respectively, each impedance is defined as follows;

$$Z_0 = \sqrt{\frac{\mu_0}{\varepsilon_0}} \quad (1)$$

$$Z_1 = \sqrt{\frac{\mu_{r1}}{\varepsilon_{r1}}}\tanh(\gamma_1 d_1) \quad (2)$$

where μ_0 and ε_0 are the permeability and permittivity of air (or vacuum), while μ_{r1} and ε_{r1} are the relative permeability and permittivity of the absorber with a thickness d_1, respectively. A propagating constant, γ_1, of an EM wave with its wavelength of λ in the absorber can be expressed as[4),5]

$$\gamma_1 = j\frac{2\pi}{\lambda}\sqrt{\mu_{r1}\varepsilon_{r1}} \quad (3)$$

which denotes that the amount of an EM wave absorbed in the material increases with an increasing $\sqrt{\mu_{r1}\varepsilon_{r1}}$ value. Thus, a perfect impedance matching, $Z_0 = Z_1$, allows EM waves to propagate from the free space to the inside of the absorber without any reflection. To establish the $Z_0 = Z_1$ condition, μ_{r1} and ε_{r1} are required to be equal. Accordingly, it is obviously desirable for an EM wave absorber to have the electromagnetic property of $\mu_{r1} = \varepsilon_{r1}$ as well as very large μ_{r1} and ε_{r1} which can lead to large energy loss characteristics.[5),6]

To fulfill this requirement as an EM wave absorber in the frequency range of 0.1–10 MHz, the fabrication of ceramic composites has been made for the combinations between magnetic and ferroelectric oxides.[7),8] In the studies of the ceramic composites, $Ni_{0.3}Zn_{0.6}Cu_{0.2}Fe_{1.96}O_4$ + $BaTiO_3$[7] and $N_{0.3}Zn_{0.5}Cu_{0.2}Fe_{1.9}O_4$ + $Pb(Zr,Ti)O_3$,[8] CuO was added to NiZn ferrites with $\mu_r \approx 1000$ in order to allow low-temperature sintering for the manufacture of multi-layer devices. CuO assisted effectively the densification of the composite samples at 900°C but concurrently lowered the μ_r values to be ~300. A reduction in μ_r in such composite system is inevitable because some non-magnetic material must be introduced to give the $\mu_r = \varepsilon_r$ condition.

Among the NiZn ferrites with various Ni/Zn ratios, the $Ni_{0.3}Zn_{0.7}Fe_2O_4$ sample shows a maximum μ_r value at room temperature.[9] Therefore, a ceramic composite of $Ni_{0.3}Zn_{0.7}Fe_2O_4$–$BaTiO_3$ was considered to be the most promising combination in which the $\mu_r = \varepsilon_r$ condition could be satisfied. Based on the mixture rule of Lichtenecker,[10] the $\mu_r = \varepsilon_r$ condition should be attained for a mixing ratio of $Ni_{0.3}Zn_{0.7}Fe_2O_4$:$BaTiO_3$ = 75:25

† Corresponding author: K. Abe; E-mail: kazuabe@eng.hokudai.ac.jp

vol% with $\mu_r \fallingdotseq \varepsilon_r \fallingdotseq$ ~200 if no reaction between them occurred under a fabrication condition. However, no detailed examination has been conducted for the ceramic composites with the mixing ratio of $Ni_{0.3}Zn_{0.7}Fe_2O_4$:$BaTiO_3$ = 100:0–75:25 vol%. Therefore, in this study, we have focused on the fabrication of the $Ni_{0.3}Zn_{0.7}Fe_2O_4$–$BaTiO_3$ (NZ ferrite-BT) composites with the mixing ratios of 0–25 vol% BT and examined the effects of solid phases and microstructure changes on, especially, the dielectric properties of the resulting ceramic composites.

2. Experimental

A NZ ferrite powder was prepared by a conventional solid state reaction. Fixed amounts of commercially available raw materials of NiO, ZnO, and Fe_2O_3 (Wako Pure Chemical Industries, Ltd.) were mixed as a slurry in a plastic container with zirconia balls for 12 h to obtain a given ferrite composition of $Ni_{0.3}Zn_{0.7}Fe_2O_4$. A mixed and dried powder was calcined at 1000°C for 4 h in air and then ground into a fine starting powder less than 1 μm. Given amounts of the NZ ferrite powder thus prepared and a commercially available $BaTiO_3$ powder (Sakai Chemical Industry Co., Ltd., $d_{ave.}$ = 0.5 μm and tetragonal phase) were mixed in the same manner as that described above to obtain composite powders with 1, 3, 5, 8, 10, 15 and 25 vol% BT mixing ratio (These samples are referred to as 1 BT, 3 BT, 5 BT, 8 BT, 10 BT, 15 BT and 25 BT composites, respectively). Green compacts of the composite powders formed by a uniaxial pressing at 50 MPa were sintered in air under various conditions (1200–1275°C for 2–48 h). The sintered samples were characterized by density measurement (Archimedes method), solid phase identification with X-ray Diffractometer (XRD: Rigaku Co., Rint 2200), microstructure observation with Scanning Electron Microscope (SEM: JEOL Ltd., JSM–6300F), and element analysis with Energy Dispersive X-ray Spectrometer (EDS: JEOL Ltd., JSM–6390LVS). Furthermore, electrical properties were evaluated for bulk composite samples coated with Ag electrodes. Dielectric permittivity (ε_r) was measured with an impedance analyzer (Agilent 4285A). An electrometer (ADCMT 8340A) equipped with a Direct current (DC) supply (Agilent E3649A) was used to measure the Current-Voltage (*I–V*) characteristic and DC resistivity by the 2-probe or 4-probe method. The magnetic permeability (μ_r) was measured with a RF material analyzer (Agilent E4991A) for a troidal disk sample with outer and inner diameters of 19 mm and 9 mm, respectively.

3. Results and discussion

3.1 Changes in ε_r, solid phase and microstructure with BT ratio

In our preliminary examination, we had found that the ceramic composites with the BT ratio ranging from 15 to 35 vol% showed considerably higher ε_r values than those calculated from the Lichtenecker's mixture formula.[10] A detailed study was then conducted for the composites with lower BT ratios. A change in measured ε_r with BT ratio is shown in **Fig. 1** for the NZ ferrite-BT composites obtained by sintering at 1250°C for 4 h. A broken line indicates a ε_r change for a serial mixture of the NZ ferrite and BT phases, which could be calculated from Lichtenecker's formula using the reference ε_r values of 20 and 3000 for the NZ ferrite and BT phases, respectively. It is obvious that the measured ε_r steeply increases toward 5 vol% BT, above which it slightly decreases with an increasing BT ratio.

The XRD results of these NZ ferrite-BT composites are shown in **Fig. 2**. It is noticed that two types of solid phase were newly formed during sintering at 1250°C. A solid phase marked with

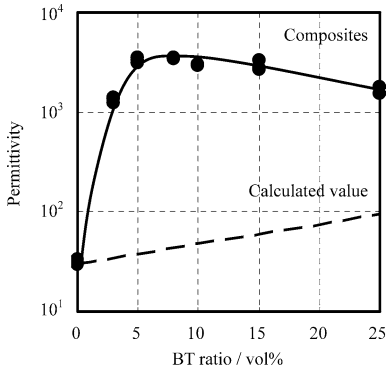

Fig. 1. Permittivity change of NZ ferrite-BT composites with BT ratio.

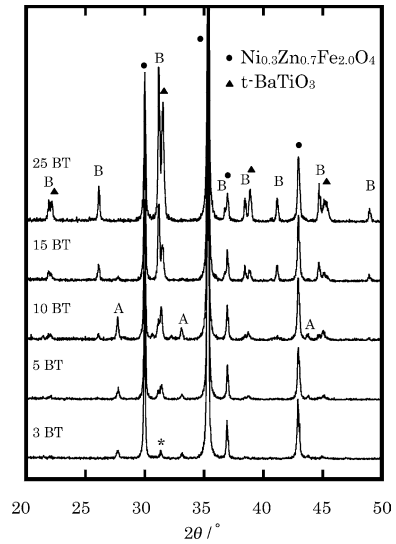

Fig. 2. Phase change of NZ ferrite-BT composites with $BaTiO_3$ ratio.

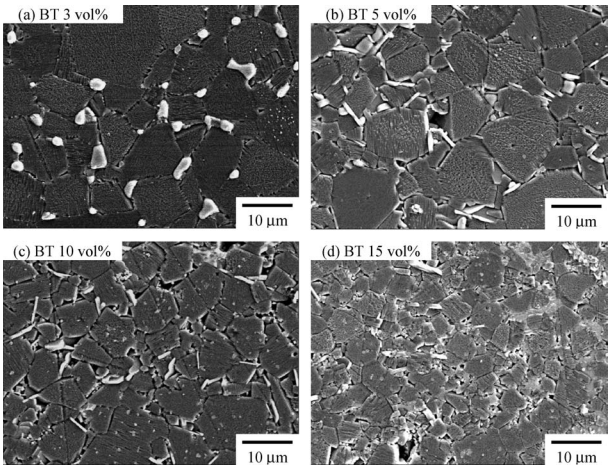

Fig. 3. SEM images of thermally etched composites with 3–15 BT.

"A" can be detected for 3–15 BT composites with its maximum peak intensity at 10 vol% BT. On the contrary, XRD peaks marked with "B" clearly appear from the 5 vol% BT composite, and their peak intensities considerably increase for the 25 vol% BT composite. The microstructure evolution with BT ratio can be seen in **Figs. 3** and **4**. The microphotographs of thermally

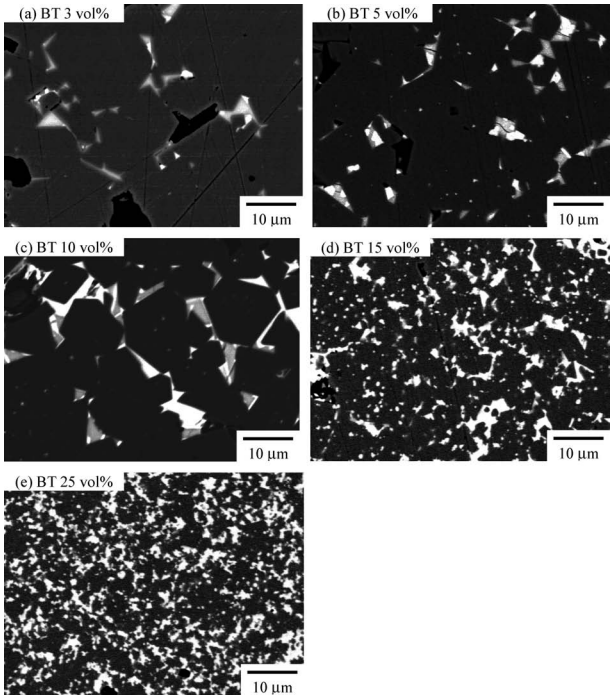

Fig. 4. BSEM images of polished composites of (a) 3 BT, (b) 5 BT, (c) 10 BT, (d) 15 BT and (e) 25 BT.

Table 1. Composition of the A-phase in Each Sample

BT (vol%)	Ba	Fe	Ti	Zn	Total
3	0.298	0.629	0.029	0.037	0.993
5	0.333	0.588	0.037	0.026	0.984
8	0.316	0.588	0.045	0.036	0.985
10	0.299	0.582	0.063	0.026	0.970

Ti content tended to increase with an increasing amount of BT mixing ratio.

Table 2. Compositional Change of h-BT in Each Composite

BT (vol%)	Ba	Fe	Ti	Zn	Fe/(Fe + Ti)	Ni
3	0.514	0.359	0.047	0.057	0.884	0.023
5	0.505	0.190	0.250	0.040	0.432	0.015
8	0.508	0.179	0.263	0.035	0.405	0.015
10	0.496	0.169	0.300	0.025	0.360	0.010
15	0.505	0.167	0.281	0.031	0.373	0.016

Fe/(Fe + Ti) ratio in h-BT was found to decrease with an increasing amount of BT

etched samples (Fig. 3) reveal that the grain size of the NZ ferrite matrix gradually decreases with an increasing BT ratio. Back-scattered electron microscopy (BSEM) images of the polished samples (Fig. 4) represent light gray or white grains which might be secondary phases produced by the reaction between the NZ ferrite and BT particles during sintering.

In order to find out what these newly formed phases "A" and "B" could be, the compositional analysis with EDS was conducted for several compositions. **Tables 1** and **2** indicate the average values of each element in the "A"-phase and "B"-phase,

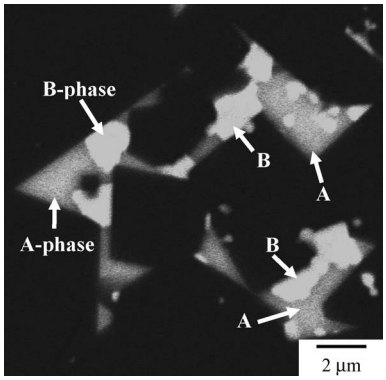

Fig. 5. A highly magnified BSEM image of 10 BT composite.

respectively, with a highly magnified image of each phase in **Fig. 5**. Based on the detailed comparative inspection of the data on many compounds reported in the BaO–TiO_2[11] and BaO–Fe_2O_3 binary systems[12] and the BaO–TiO_2–Fe_2O_3 ternary system[13] with the results obtained in this study (the XRD profiles and chemical composition analysis given in Tables 1 and 2), both phases could be identified. That is, the "A"-phase was proved to be the hexagonal $BaFe_2O_4$ solid solution in which the (Ti, Zn, Ni) cations could be incorporated in the Fe^{3+} site, and the "B"-phase was the hexagonal $BaTiO_3$ (h-BT) type compound containing considerable amounts of Fe. It is known that an extensive solid solution between $BaTiO_3$ and $BaFeO_{2.5}$ with the hexagonal $BaTiO_3$ structure is formed,[12] in which both Fe^{3+} and Fe^{4+} cations could be substituted for Ti^{4+} cations with the general formula $BaTi_{1-x-y}Fe^{3+}_xFe^{4+}_yO_{3-x/2}$. The substitution of Fe^{3+} for Ti^{4+} is accompanied by the formation of oxygen vacancies up to a limited composition of $BaFe_{0.67}Ti_{0.33}O_{2.67}$. For the solid solutions with the [Fe]/[Fe + Ti] ratio higher than 0.67, further incorporation of Fe occurs as Fe^{4+} while the oxygen vacancy concentration remains constant.[12] In the present study, a very high Fe content in the 3 vol% BT composite (Table 2) with the corresponding XRD peak shifting toward a higher 2θ (marked with * in Fig. 2) would be explained by the incorporation of a much larger amount of the Fe cation as Fe^{4+}. Above 5 vol% BT, the XRD peak intensity of the h-BTss phase, in which a 40–50% of the Ti-site available in the structure was replaced by Fe, Zn and Ni, correspondingly increases with an increasing BT ratio (Fig. 2). The coexistence of tetragonal $BaTiO_3$ (t-BT) and h-BT phases in the sintered composites might be partly due to the aggregation of the dispersed BT particles during the powder mixing process or the formation of core-shell type BT particles.

3.2 Formation of a liquid phase and related changes

The presence of wedge-shaped regions in some composites (Fig. 4) suggested that a liquid phase would form during sintering at 1250°C and consolidate along the NZ ferrite grains during the cooling process. So a detailed examination on the microstructure evolution of the 10 vol% BT composites was conducted as a function of sintering temperature or sintering time. Typical BSEM images of such composites are given in **Fig. 6** where wedge-shaped regions are irregularly distributed in all the samples, indicating that a liquid phase was already produced at 1200°C and the area of the wedge-shaped regions were extended with increasing sintering temperature and time. The corresponding phase changes could be confirmed from the XRD patterns

shown in **Fig. 7**. A slight change was detected for the XRD peak intensity of the $BaFe_2O_4$ss phase in the 10 vol% BT composites obtained under different sintering conditions. On the contrary, the relative amount of the h-BTss vs. t-BT phases changed considerably depending on sintering conditions. That is, the h-BTss/t-BT intensity ratio correspondingly increased with increases in sintering temperature and sintering time at 1200°C (4 h → 12 h → 48 h). The location of the h-BTss grains could be detected from highly magnified BSEM observation of the composite samples. As clearly shown in a representative BSEM image in Fig. 5, the h-BTss grains (the "B"-phase in Fig. 5) were definitely involved in the wedge-shaped regions where the remaining sharply-edged portions were found to be composed of $BaFe_2O_4$ss (the "A"-phase). These results revealed that a liquid phase could form in the pseudobinary eutectic system of $BaFe_2O_4$ss with a lower melting temperature ($BaFe_2O_4$ itself congruently melts at 1420°C[14]) and h-BTss. Therefore, the deposition and growth of the h-BTss grains would mainly occur in a liquid phase during sintering, while the $BaFe_2O_4$ss grains consolidate during the cooling process, which resulted in the specified microstructures of the composites fabricated in this study.

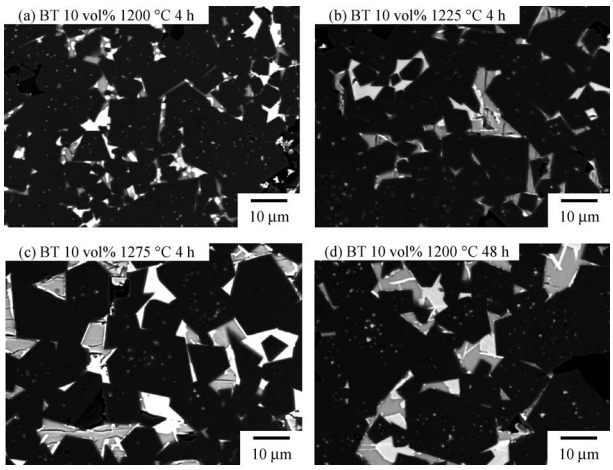

Fig. 6. Microstructure evolution of 10 BT composites sintered under different conditions.

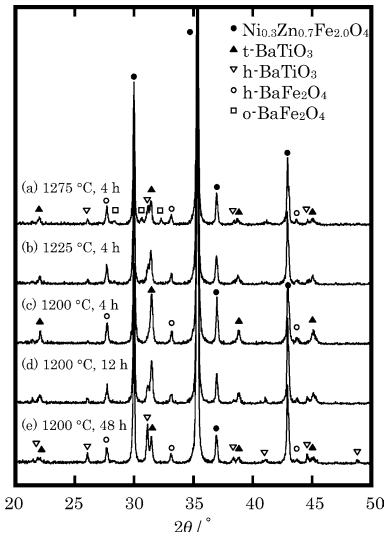

Fig. 7. Phase change of 10 BT composites with sintering conditions.

As for the formation of a liquid phase, it was noticed that the amount of the liquid phase formed during sintering was dependent on the BT ratio in the composites. A decreasing fraction of the wedge-shaped regions with an increasing BT ratio could be recognized by comparing the BSEM images between 10 BT, 15 BT and 25 BT composites shown in Fig. 4(c), (d) and (e), which indicated that the amount of a liquid phase was gradually reduced with an increasing BT ratio. As a result of a reduced amount of a liquid phase, the formation of the $BaFe_2O_4$ss and h-BTss phases should be considerably suppressed. Contrary to this relationship, however, the increasing production of the h-BTss phase was observed for the 15 BT and 25 BT composites (Fig. 2). The intensified production of the h-BTss phase in these composites with few or no liquid phase would be explained by the solid state reaction between t-BT and NZ ferrite particles during sintering. Thus the formation process of the h-BTss grains might be different depending on the t-BT content in the present composite system.

3.3 Possible causes leading to large ε_r

Three possible causes were considered for substantially high ε_r values observed in the composites with the BT ratio more than 3 vol% (Fig. 1). These are (1) the formation of new compounds having very high ε_r, (2) the formation of a capacitive barrier layer at grain boundaries, and (3) the occurrence of electron hopping between Fe^{2+} and Fe^{3+} in the NZ ferrite phase.

The fractional solid phases present in the composites sintered at 1250°C for 4 h are given in **Fig. 8** for the purposes of comparison with the ε_r change in Fig. 1. If a steep ε_r increase in a composition range up to 5 BT is due to the formation of the $BaFe_2O_4$ss phase, it could not reasonably explain the substantially large ε_r values of the 15 BT and 25 BT samples. Therefore, the remarkable increase in ε_r could not be attributed to such a change of the newly formed secondary phases with BT content. However, as for the formation of the $BaFe_2O_4$ss phase, a liquid phase was found to be produced during sintering for a limited BT range of 3%–15%. A contribution of such a liquid phase formed during sintering, capacitive layers might be produced along grain boundaries of NZ ferrite. If a material consisted of electrically conductive grains surrounded by an insulating layer, then it has a very large effective ε_r and similar properties to those of varistors.[15] In order to elucidate whether this kind of barrier-layer structure has been constructed or not, the *V–I* property under the DC field was measured by the 4-probe method for the composites. **Figure 9** shows the *V–I* relationships of some composites sintered at 1250°C for 4 h. The each composite sample reveals a linear correlation between I_{DC} and V_{DC}, from which an exponent

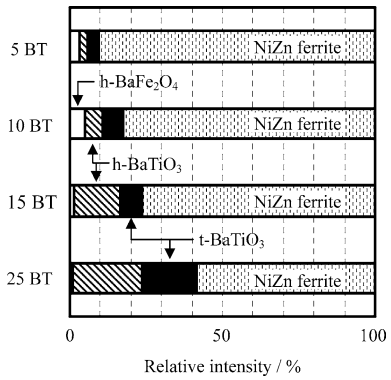

Fig. 8. Fractional phase change in each composite.

α in the relation $I = kV^{\alpha}$ [16] was evaluated to be $\alpha = 1.0$ for all the samples and also a DC bulk resistivity to be $\rho/\Omega\cdot cm = 6.3 \times 10^3$, 3.4×10^1, 4.4×10^1, 2.3×10^1 for 0 BT, 5 BT, 10 BT and 15 BT, respectively. The α value and substantially low values of the bulk resistivity of the composite samples indicated that capacitive boundary layers were not produced in the present composite system.

To examine the effect of electron hopping in the NZ ferrite, which could occur by the incorporation of a tetravalent cation such as Ti^{4+} into Fe^{3+}-site in the spinel structure,[17] on the electrical properties of the composites, the Ti concentration in the NZ ferrite matrix phase was measured by EDS analysis for each composite sample. The result is given in **Fig. 10** where each Ti concentration, which was derived by assuming that measured Ti ions occupied the octahedral B-sites, is plotted against the corresponding BT mixing ratio. It should be noticed that the Ti concentration was substantially low in all the composite samples and gradually increased to reach as high as 3.0 at% for the 15 BT composite. Based on this result, several Ti-doped NZ ferrite samples were separately fabricated by sintering at 1250°C for 4 h to elucidate the effect of the Ti-doping on their electrical properties. **Figure 11** shows DC resistivity changes for the composites and Ti-doped ferrites as a function of the Ti concentration in each sample. Both curves indicated that the substitution of a small amount of the Ti^{4+} cations caused a DC resistivity change by two or three orders of magnitude lower than those of the original Ti-undoped samples.

There have been many studies on the effect of the Ti^{4+} cation substitution on the magnetic, electric and dielectric properties of spinel ferrites.[17–20] According to these studies, the Ti^{4+} substitution should lead to the reduction in their electrical conductivity and dielectric constant, which was opposite to the result of this study. However, those changes already reported were observed for the ferrites containing substantial amounts of Ti^{4+} (mostly more than 10 mol%), which was fairly different from the Ti concentration in the present NZ ferrite samples. The conductivity mechanism of the NZ ferrite family is believed to be electron hopping between ions of the same type on equivalent sublattice, Fe^{3+} and Fe^{2+}. For the NZ ferrite, it is known that the resistivity of the $Ni_{0.3}Zn_{0.7}Fe_{2+\delta}O_{4-x}$ ferrite shows a very drastic change depending on the iron content δ. With a very small positive δ, the insulating state of the stoichiometric sample of $\delta = 0$ could be converted to the condition for n-type electron hopping by the presence of some Fe^{2+}, resulting in lowering in the resistivity by several orders of magnitude.[21] Probably, the similar situation would occur when a small amount of Ti^{4+} is incorporated in the NZ ferrite fabricated in this study. That is, the lowering in the DC resistivity observed for samples containing small amounts of Ti could be closely associated with the creation of Fe^{2+} by the Ti^{4+} substitution.

In addition to the DC resistivity, ε_r changes with Ti concentration incorporated in the NZ ferrite phases were examined for the Ti-doped samples obtained in this study. The results are shown in **Fig. 12**. It is clearly seen that increasing ε_r behaviors observed for the composites and Ti-doped ferrite samples with an increasing Ti concentration are very similar to those of the DC resistivity of the corresponding samples, suggesting that electron hopping conduction induced by a small amount of Ti-doping in the ferrite could be responsible for the increases in ε_r. Decreasing ε_r values after each ε_r maximum could be explained by the following changes; a gradual lowering in the sinterability with an increasing amount of Ti-doping for the BT-free NZ ferrite samples and a relative reduction of the Ti-doped NZ ferrite phase

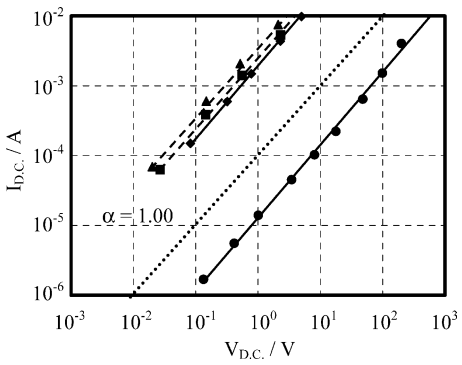

Fig. 9. $V_{D.C.}$ -$I_{D.C.}$ characteristic of NZ ferrite-BT composites. (–●– 0 BT, -■- 5 BT, –◆– 10 BT, -▲- 15 BT).

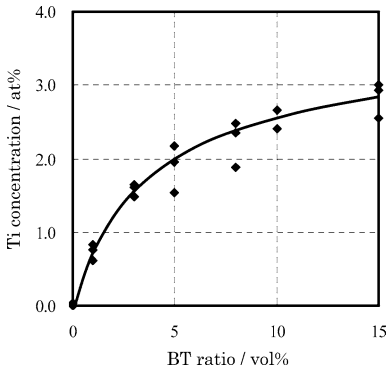

Fig. 10. Relationship between Ti concentration in NZ ferrite and BT mixing ratio.

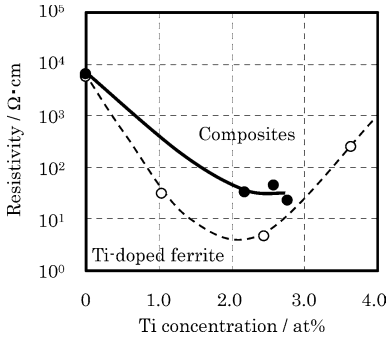

Fig. 11. DC resistivity changes with Ti concentration for Ti-doped ferrite and composites.

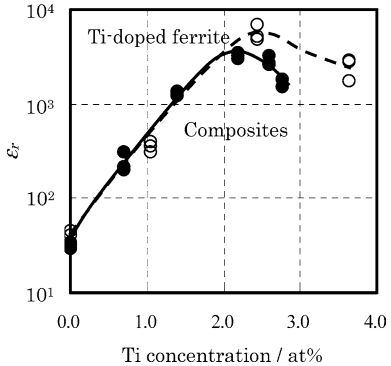

Fig. 12. ε_r changes with Ti concentration for Ti-doped ferrite and composites.

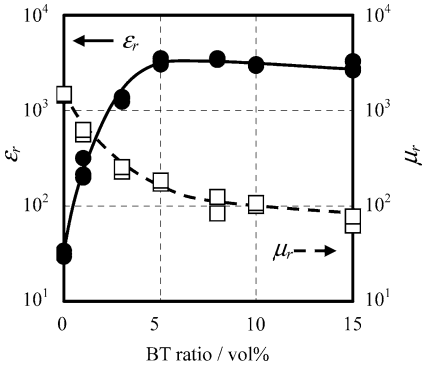

Fig. 13. Changes in ε_r and μ_r with BT ratio for NZ ferrite-BT composites.

which should contribute to the enhanced ε_r character for the composites samples with an increasing Ti-doping concentration (the relative phase change is given in Fig. 8 as a function of BT mixing ratio). Thus, a steep increase in ε_r for the composite samples containing 3–5 vol% BT could be predominantly attributed to the electron hopping between Fe^{2+} and Fe^{3+} in the matrix NZ ferrite phase, which were caused by the incorporation of a small amount of Ti^{4+} into the Fe^{3+}-site in the spinel ferrite.

Finally, dependences of ε_r and μ_r on the BT ratio are presented in **Fig. 13** for the present composite system. The rate of decreasing μ_r for the composites is faster than the calculated rate, which might be due to the Ti-substitution and production of secondary phases with low μ_r. Further studies will be conducted to make the ε_r and μ_r changes of composites more controllable.

4. Conclusion

The ceramic composites for which 3–25 vol% $BaTiO_3$ (BT) particles were dispersed in a ferrite matrix phase of $Ni_{0.3}Zn_{0.7}Fe_{2.0}O_4$ (NZ ferrite) were fabricated from powder mixtures at 1250°C and the effects of solid phases and microstructure changes on the electrical properties were studied as a function of the BT ratio. A remarkable feature of this composite system was a steep increase in ε_r for the samples containing small amounts of BT up to 5 vol%. Detailed examination on the solid phases and microstructure changes with BT ratio revealed the production of a liquid phase during sintering in a limited BT ratio of 3–15 vol% and the corresponding formation of secondary $BaFe_2O_4$ss and hexagonal BTss phases. However, these changes originated from a reaction between NZ ferrite and BT brought little effect on the substantially enhanced ε_r. From electrical property evaluations such as *V–I* characteristic of the composites and DC resistivity change with the Ti concentration in the NZ ferrite, a remarkably increasing ε_r was found to predominantly come from the electron hopping between Fe^{2+} and Fe^{3+} in the matrix NZ ferrite, which would be caused by the substitution of a small amount of Ti^{4+} for the Fe-sites in the spinel structure.

Reference

1) K.Yamagiwa, F. Zhang, T. Sato, K. Yamasawa and Y. Miura, *IEEE Trans. Magne.*, 41[10], 3571–3573 (2005).
2) N. C. Joshi, A. Verma, N. Kumar, S. Kumar O. B. and S. S. Islam, *Defence Science Journal*, 57[4], 471–480 (2007).
3) V. M. Petrov, V. V. Gagulin, *Inorganic Materials*, 37[2], 93–98 (2001).
4) M. P. Horvath, *J. Magn. Magn. Mater.*, 215–216, 171–183 (2000).
5) Y. Naito, K. Suetake, *IEEE Transactions*, MIT-10[1], 65–72 (1971).
6) Y. Naito, H. Anzai, T. Mizumoto and M. Takahashi, *Proc 1993 IEEE Int. Symp. EMC*, *Dallas*, *TX*, 254–259 (1993).
7) X. Qi, J. Zhou, Z. Yue, Z. Gui and L. Li, *J. Magn. Magn. Mater.*, 269, 352–358 (2004).
8) N. Kitahara and T. Mizumoto, *IEICE Trans C*, J86-C[4], 450–456 (2003).
9) A. J. Moulson and J. M. Herbert, "Electroceramics, 2nd ED." John Wiley & Sons Ltd., Chichester (2003) pp. 492–494.
10) K. Chung, C. M. Lin, S. F. Wang, S. T. Lin and C. F. Yang, *Mater. Lett.*, 61[3], 757–760 (2007).
11) J. Nowotny and M. Rekas, *Key Eng. Mater.*, 66 & 67, 45–144 (1992).
12) I. E. Grey, C. Li, L. M. D. Cranswick, R. S. Roth and T. A. Vanderah, *J. Solid State Chem.*, 135, 312–321 (1998).
13) T. Siegrist and T. A. Vanderah, *Eur. J. Inorg. Chem.*, 1483–1501 (2003).
14) S. Meriani, *Acta Crystallogr. B*, 28, 1241–1243 (1972).
15) A. J. Moulson and J. M. Herbert, "Electroceramics, 2nd ED." John Wiley & Sons Ltd., Chichester (2003) pp. 326–329.
16) A. J. Moulson and J. M. Herbert, "Electroceramics, 2nd ED." John Wiley & Sons Ltd., Chichester (2003) pp. 150–155.
17) A. M. M. Farea, S. Kumar, K. M. Batoo, A. Yousef and C. G. Lee, *J. Alloys Compd.*, 469, 451–457 (2009).
18) T. M. Meaza, S. M. Attiab and A. M. Abo El Ata, *J. Magn. Magn. Mater.*, 257, 296–305 (2003).
19) S. S. Suryavanvanshi, R. S. Patil, S. A. Patil and S. R. Sawant, *J. Less-Common Met.*, 168, 169–174 (1991).
20) C. Prakash and J. S. Baijal, *J. Less-Common Met.*, 107, 51–57 (1985).
21) A. J. Moulson and J. M. Herbert, "Electroceramics, 2nd ED." John Wiley & Sons Ltd., Chichester (2003) pp. 496–501.